Ionics (2013) 19:1067–1075
DOI 10.1007/s11581-013-0926-x

SHORT COMMUNICATION

Thermal analysis, Raman spectroscopy and complex impedance analysis of Cu^{2+}-doped KDP

Houda Ettoumi · Youping Gao · Mohamed Toumi · Tahar Mhiri

Received: 16 March 2013 / Revised: 2 May 2013 / Accepted: 26 May 2013 / Published online: 13 June 2013

Abstract Raman spectroscopy and differential thermal analysis (DTA) and thermogravimetric analysis have been carried out on Cu-doped KH_2PO_4 (Cu-KDP). X-ray diffraction powder data reveal that the structure of the KDP crystal does not change with the additive Cu^{2+} ion. DTA analysis and Raman study of Cu-KDP as a function of temperature reveal that this compound undergoes two phase transitions at about Ttr =453 and 473 K. The electrical conductivity measurements on polycrystalline pellet of Cu-KDP (5) are performed from room temperature (RT) up to 495 K. Only one phase transition is observed at 470 K. The activation energy in the migration is 0.42 eV in the temperature range from RT to 470 K. For temperature above 470 K, the activation energy of the superprotonic phase is 1.87 eV.

Keywords Phase transformation · Raman spectroscopy · Dielectric properties

Introduction

The KDP family compounds (MH_2PO_4; M=K, Cs, Rb, NH_4) are interesting for many reasons [1–6]. In particular, CsH_2PO_4 (CDP) as a fuel cell electrolyte at temperatures so-called superprotonic behaviour present an abrupt, several-order-of-magnitude jump in its proton conductivity upon heating above the temperature Ttr≈508 K[7]. It is demonstrated that the above-mentioned proton conductivity enhancement is associated with a polymorphic phase transition from its room temperature monoclinic ($P2_1/m$) phase to a high-temperature dynamically disordered cubic (Pm-3m) CDP modification [8]. Interestingly, the RbH_2PO_4 (RDP) compound also exhibits a superprotonic transition at 566 K, although at room temperature RDP is not monoclinic as CDP, but tetragonal ($I\bar{4}2d$). Using synchrotron X-ray studies, Botez et al. [8] demonstrated that heating RDP towards its superprotonic transition leads to an intermediate temperature (Ttr =383 K) change of the RDP tetragonal phase into a monoclinic modification, isomorphic (crystallographically identical) to the monoclinic CDP phase. There is another phosphate, $NH_4H_2PO_4$, which crystallizes at room temperature in tetragonal space group $I\bar{4}2d$ and upon heating does not show an abrupt enhancement of its proton conductivity [9].

Much less is understood about the structural, chemical and physical property changes that occur in KH_2PO_4 (KDP) upon heating from room temperature toward its melting point. Thermal events observed around Ttr =458 K, for example, have been attributed by some authors to a polymorphic phase transition at an intermediate-temperature KDP modification [10], while others have claimed that the behaviour at Ttr was in fact due to chemical changes, such as dehydration and onset of partial polymerization of the room temperature of tetragonal KDP phase [11, 12].

Previous investigations of the structural changes of KDP have been devoted, in the past few years, to understand the exact nature of this transition in KDP, which remained a controversial subject. Using X-ray diffraction measurements, Itoh et al. [13] concluded that on heating through 460 K, the crystal system changed from tetragonal to monoclinic, space group $P2_1$ or $P2_1/m$. The lattice parameters at 468 K were given as a=7.47 Å, b=7.33 Å, c=14.49 Å, $\alpha=\beta=90°$ and $\gamma=92.2°$. The spots in the Weissenberg photograph at 468 K were only consistently indexed by assuming a twin structure in the monoclinic phase appearing above 460 K. The complete assignment of the reflections was difficult to do, and until now detailed

H. Ettoumi (✉) · M. Toumi · T. Mhiri
Laboratoire de L'Etat Solide (LES), Faculté des Sciences de Sfax, Université du Sfax, Route de Soukra Km 3.5, BP 802, 3018, Sfax, Tunisia
e-mail: ettoumihouda@yahoo.fr

Y. Gao
Laboratoire des Oxydes et Fluorures, Université du Maine, CNRS UMR 6010, Avenue O. Messiaen, 72085 Le Mans, France

Table 1 Different concentrations determined by atomic absorption analysis, with a weight error of 2 %

	Concentration of samples (mg/g)
Cu-KDP (1)	0.57
Cu-KDP (2)	0.75
Cu-KDP (3)	1.21
Cu-KDP (4)	2.49
Cu-KDP (5)	3.02

structural analyses including atomic coordinates have not been done [11]. Moreover, it has been reported that the monoclinic phase of KDP is metastable at temperatures below Ttr and that it reverts to the stable tetragonal phase after being kept for some days in air at room temperature [10, 12–14]. Very recently, temperature-resolved synchrotron X-ray studies have demonstrated that heating KDP towards its superprotonic transition leads to an intermediate temperature (Ttr =463 K), where the KDP tetragonal phase changes into a monoclinic phase, the same as both isomorphic monoclinic RDP and CDP [15]. Moreover, they observed that monoclinic KDP is stable up to 508 K and indicated that a monoclinic ($P2_1/m$)–cubic (Pm3m) transition upon further heating similar to the one responsible for the superprotonic behaviour of CDP and RDP is not precluded. They concluded that the reported lack of superprotonic behaviour in KDP [16] was most likely due to ion size effects and not due to crystal structure considerations.

In view of these results, it appears that further investigations aimed to clarify the structural changes undergone by KDP upon heating above Ttr are worth carrying out.

It is well known that the presence of a small amount of impurities can considerably influence the growth habit, optical properties and dielectric properties of KDP crystals [17–21].

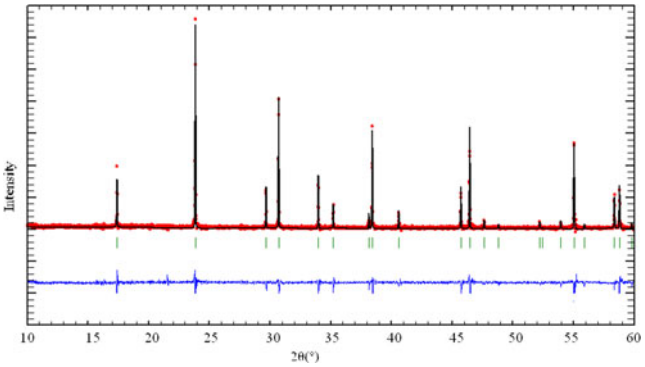

Fig. 2 The Pawley refinement of the lattice parameters of Cu-KDP (5). The *point symbols* represent the observed diffraction pattern, the *solid lines* represent the calculated pattern and the *curves at the bottom* of the figure represent the difference between the observed and calculated patterns. The *short vertical lines* mark the positions of possible Bragg reflections

Due to various physicochemical properties, impurities can be selectively incorporated at the surface of the crystal layer and into the kink sites. The presence of metallic impurities may form both isolated and interstitial defect centres [22].

This work presents the evolution of the Raman spectra of single crystal of pure KDP and Cu^{2+}-doped KDP (Cu-KDP) when the temperature is raised from 303 to 503 K. Raman scattering method has been successfully used to reveal structural information about a wide variety of inorganic compounds: phosphate solid acids [23, 24] and sulfate [18, 25, 26]. In particular, Raman spectroscopy is used to demonstrate the effect of heating on the partial decomposition of KDP [25, 27]. Thus, this method is suitable for the present investigation, which presents also the influence of bivalent Cu^{2+} impurity ions on the electrical properties.

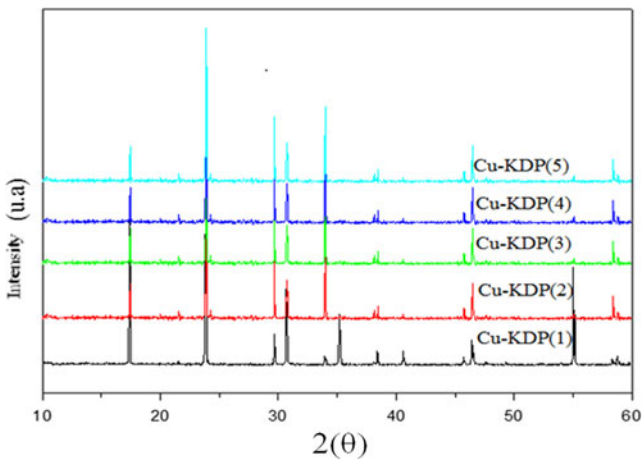

Fig. 1 The XRD patterns of Cu-KDP (1), Cu-KDP (2), Cu-KDP (3), Cu-KDP (4) and Cu-KDP (5)

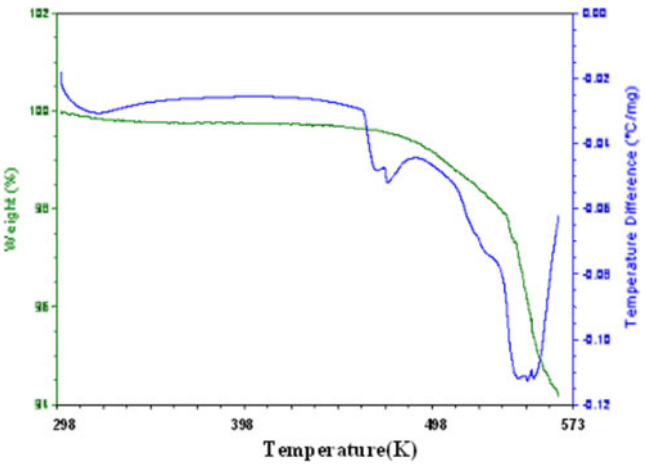

Fig. 3 Thermograms of DSC and TGA for Cu-KDP in the room temperature −573 K range

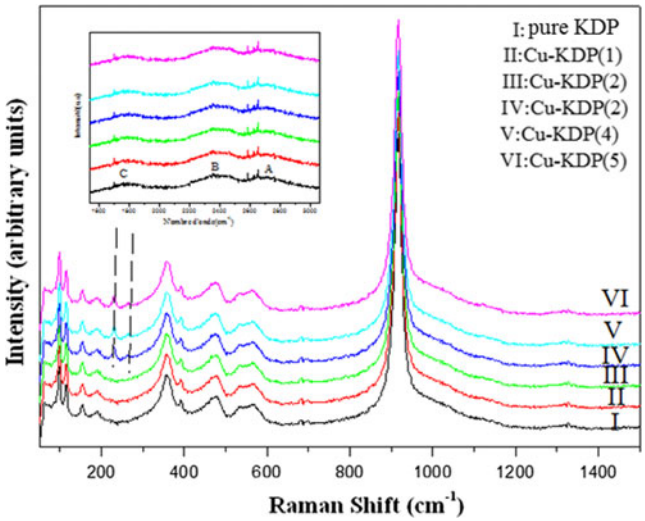

Fig. 4 Raman spectra for the pure KDP, Cu-KDP (1), Cu-KDP (2), Cu-KDP (3), Cu-KDP (4) and Cu-KDP (5) at room temperature

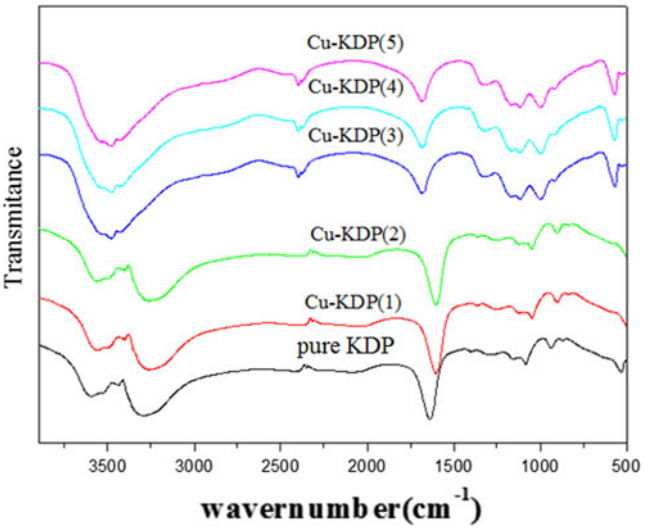

Fig. 5 FT-IR spectra recorded for the pure KDP, Cu-KDP (1), Cu-KDP (2), Cu-KDP (3), Cu-KDP (4) and Cu-KDP (5) at room temperature

Experimental details

Five samples, Cu-KDP (1), Cu-KDP (2), Cu-KDP (3), Cu-KDP (4) and Cu-KDP (5), were prepared. Each sample was prepared by slow evaporation of 20 ml of a saturated aqueous solution of KDP containing, respectively, 0. 5, 0.75, 1, 1.5 and 2 g of Cu $(OH)_2$. The concentration is determined by atomic absorption analysis, with a weight error of 2 % (Table 1).

Figure 1 compares the XRD patterns of Cu-KDP (1), Cu-KDP (2), Cu-KDP (3), Cu-KDP (4) and Cu-KDP (5) as well as from KDP references.

The characterization of compound is carried out from X-ray diffraction powder data. The intensities of the diffractograms are collected by using a diffractometer Bruker-AXS, type D8 with CuKα radiation ($\lambda(K_{\alpha 1})$ =1.54060 Å, $\lambda(K_{\alpha 2})$ =1.54443 Å). Diffraction intensities are measured between 10° and 60°, with a 2θ step of 0.02° for 2 s per point. The data are collected at room temperature. The unit cell parameters calculated by using the patterns matching the routine of the FULPROOF program [28] are a =7.45 Å and b =6.974 Å. Figure 2 shows the X-ray diffraction (XRD) pattern of Cu-KDP (5). All the reflection peaks of the XRD pattern of the sample are indexed in a single-phase tetragonal KDP structure with I $\overline{4}$ 2d space group [29].

Thermogravimetric (TGA) and differential thermal analysis (DTA) are performed on polycrystalline with a TGA/DTA Q600 STD TA Instruments apparatus (sample with Pt crucibles,

Table 2 Raman spectra of pure KDP, Cu-KDP (1), Cu-KDP (2), Cu-KDP (3), Cu-KDP (4) and Cu-KDP (5)

Pure KDP	Cu-KDP (1)	Cu-KDP (2)	Cu-KDP (2)	Cu-KDP (2)	Cu-KDP (2)	Assignment
116m	115m	115m	118m	118m	118m	Lattice vibrations
154m	152m	154m	159m	157m	160m	
187w	187w	187w	188w	188w	189w	
191w	191w	191w	193w	193w	193w	ν (O–H≡O)
			235m	234m	235m	Cu–O
			253m	253m	253m	
358m	357m	357m	352m	355m	354m	$\delta_s[PO_2, P(OH)_2]$
391w	390w	390w	389w	388w	388w	$\gamma_\tau P(OH)_2$
474m	469m	469m	473m	475w	473m	$\delta_r[PO_2, P(OH)_2]$
536w	529w	529w	530w	532w	533w	$\gamma_\omega P(OH)_2$
565m	563m	563w	561w	561w	561w	$\delta_{sc}[PO_2, P(OH)_2]$
916vs	916vs	916vs	914vs	914vs	914vs	$\nu_s P(OH)_2$
1,817m	1,810m	1,815m	1,759w	1,753m	1,758m	Band C
2,370m	2,369m	2,368m	2,373m	2,379m	2,383m	ν_{O-H} (band B)
2,728m	2,719m	2,720m	2,829m	2,831m	2,830m	ν_{O-H} (band A)

vs very strong, *s* strong, *m* medium, *w* weak

Table 3 Infrared spectra of pure KDP, Cu-KDP (1), Cu-KDP (2), Cu-KDP (3), Cu-KDP (4) and Cu-KDP (5)

Pure KDP	Cu-KDP (1)	Cu-KDP (2)	Cu-KDP (2)	Cu-KDP (2)	Cu-KDP (2)	Assignment
494m	492m	490m	466m	466m	463m	$\delta_r[PO_2, P(OH)_2]$
549m	546m	544m	569m	568m	568m	$\gamma_\omega P(OH)_2$
829m	829m	832m	886m	887m	886m	ν_s $P(OH)_2$
934m	928m	926m	998m	996m	996m	$\nu_{as}P(OH)_2$
1,083w	1,079w	1,071w	1,108w	1,108w	1,106w	$\delta_s(PO_2)$
1,151w	1,149w	1,134w	1,169w	1,168w	1,168w	$\delta_{as}(PO_2)$
1,288w	1,284w	1,281w	1,329w	1,329w	1,326w	$\delta_{as}(H)$
1,635s	1,631s	1,629s	1,683s	1,682s	1,681s	Band C
2,045w	2,038vw	2,032vw	–	–	–	ν_{O-H} (band B)
2,293vw	2,288vw	2,285vw	–	–	–	
2,343vw	2,339vw	2,337vw	–	–	–	
2,386vw	2,376vw	2,373vw	2,381m	2,383m	2,379m	
–	–	–	2,398m	2,394m	2,394m	
3,268s	3,264s	3,261s	–	–	–	γ (O–H)
–	–	–	3,430w	3,428w	3,428w	
3,435w	3,430w	3,425w	–	–	–	
–	–	–	3,483w	3,480w	3,483w	
3,516w	3,512w	3,513w	–	–	–	
–	–	–	3,565w	3,565w	3,565w	
3,600m	3,593m	3,592m	–	–	–	

vs very strong, *s* strong, *m* medium, *w* weak

Al_2O_3 as a reference). Thermograms are collected on 28.65-mg samples in the RT–573 K range with a heating rate of 10 K/mn under a dry nitrogen flow rate of 100 ml/mn.

Raman spectra are measured with a LABRAMHR 800 triple monochromator. The slit widths are set to maintain a resolution of approximately 3 cm^{-1}. The excitation light is 632.81 nm wavelength of He–Ne (20 mV) laser. Measurements are carried out using a microscope in an open furnace (under air, at ambient pressure) heating from 303 to 513 K. The heating rate is 10 K/mn, waiting for 1 min after stabilization of temperature, and collecting time for each spectrum is 10 s.

The infrared absorption spectrum was recorded using a pellet of sample, which was prepared by mixing 1 mg sample in a total weight (samples+KBr) of 200 mg. A Perkin-Elmer FT-IR

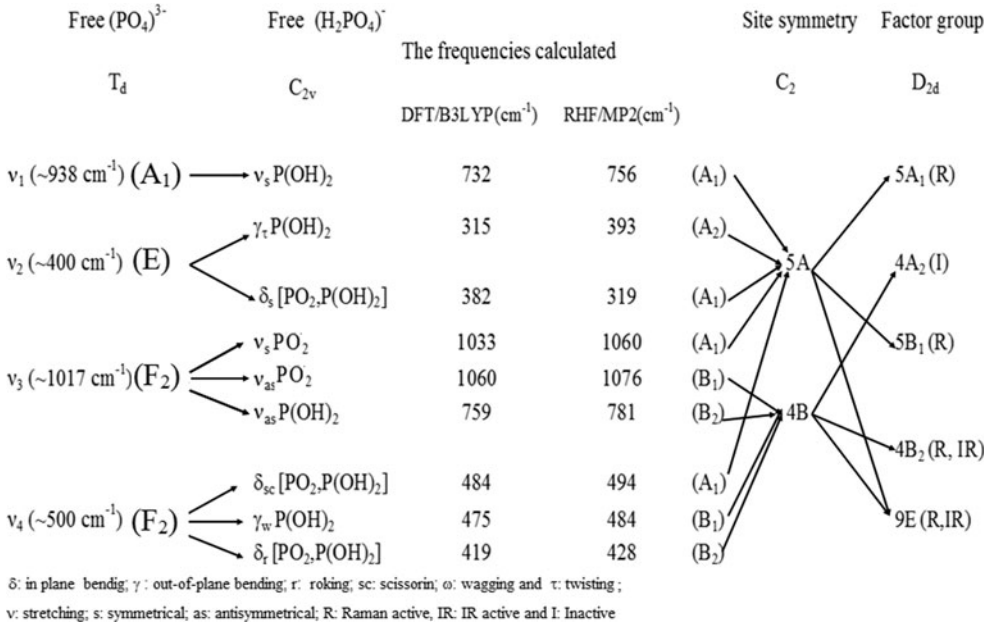

Fig. 6 Correlation scheme of internal vibration of the $(H_2PO_4)^-$ in tetragonal Cu-KDP

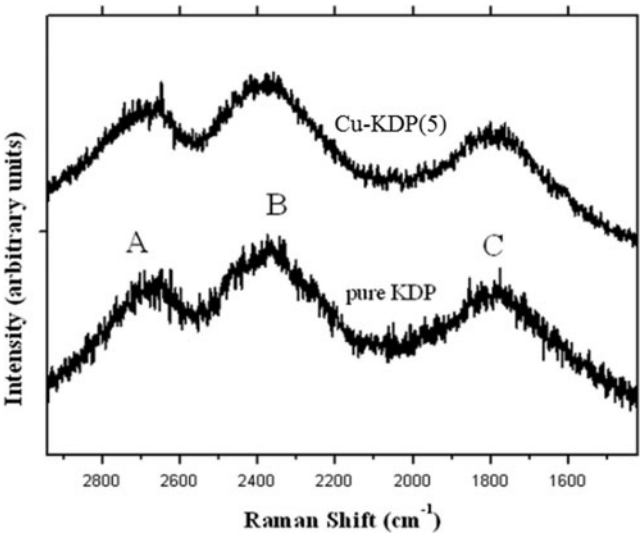

Fig. 7 ABC-type bands in the Raman spectrum for the pure and Cu-KDP (5) at room temperature

system PC spectrophotometer in the range of 4,000–400 cm^{-1} using 30 scans with 4-cm^{-1} spectral resolution was used for this purpose. A reference pellet was prepared using 200 mg KBr and has been used to correct the background.

Table 4 Wavenumbers (cm^{-1}) of the bands in the Raman spectra of Cu-KDP (5)

II T=303 K	I(a) T=453 K	I(b) T=473 K	Assignment
–	61w	64w	Lattice vibrations
–	73w	–	
–	94w	–	
–	–	–	
–	–	106w	
118m	–	–	
–	154m	155m	
152m	–	–	
182m	–	–	ν (O–H—O)
193m	–	–	Cu–O
235m	229m	230w	
253m	–	–	
		286m	
			$\delta_s[PO_2, P(OH)_2]$
354m	364m	374m	$\gamma_\tau P(OH)_2$
473w	429w	545w	$\delta_r[PO_2, P(OH)_2]$
533w	507w	604w	$\gamma_\omega P(OH)_2$
561s	572s	620vs	$\delta_{sc}[PO_2, P(OH)_2]$
	901m		$\nu_s P(OH)_2$
914s	960s	922vs	
		1,100m	$\nu_{as}(PO_2)$
	1,175m		

vs very strong, *s* strong, *m* medium, *w* weak

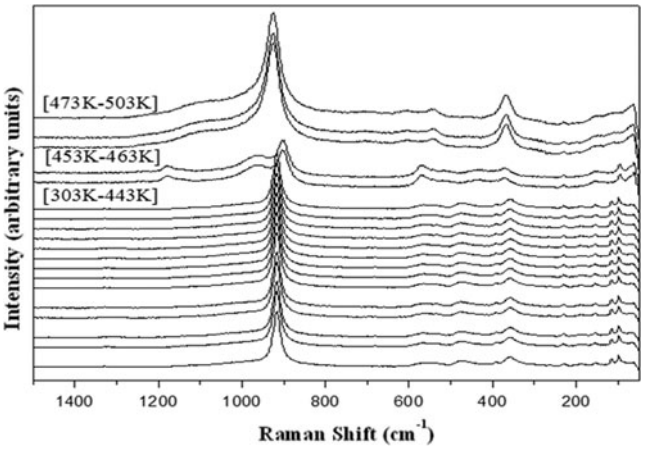

Fig. 8 Raman spectra of Cu-KDP (5) single crystal in the temperature range 303–503 K

Electrical conductivity measurements were carried out by means of impedance spectroscopy in dehydrated N_2 atmosphere in the temperature range from 315 to 495 K. The experiments were done out with ion-blocking sputtered Pt electrodes in a two-probe cell. A frequency response analyser (Solartron 1260) and a dielectric interface (Solartron 1296) were used in the frequency domain from 1 Hz to10 MHz. Before each measurement, electrochemical system linearity and stability were checked. An AC voltage of 300 mV is used, with a waiting time of 25 min for each 23-°C step (thermal equilibration). Impedance diagrams plotted in the Nyquist complex plane were fitted with a series combination of Rs and Rp//CPE elements of the Z-view 3.2c software assigned [30].

Results and discussion

DTA and TGA studies

The thermal measurement (Fig. 3) of Cu-KDP (5) reveals the presence of two high-temperature phase transitions at 462 K (189 °C) and 473 K (200 °C). Thermal gravimetric analysis shows that the transition is not related to decomposition. Significant weight loss occurred from 498 K (225 °C).

Infrared and Raman spectroscopy

The KDP crystal at room temperature may be considered as consisting of K^+ and $(H_2PO_4)^-$ ions belonging to the space group I $\bar{4}$ 2d. The H_2PO_4 groups together with atoms of K lying between them on axis z (c) create columns shifted one against the other at c/4 along the direction z. Each PO_4 group is linked with four neighbouring PO_4 groups by four hydrogen bonds lying almost exactly in the planes perpendicular to the z-axis. The local symmetry of the (H_2PO_4) tetrahedron is C_2,

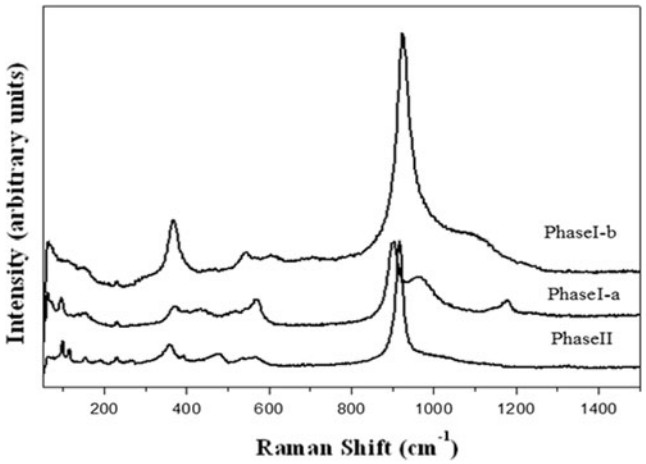

Fig. 9 Raman spectra of Cu-KDP (5) material in phase II, phase I-a and phase I-b

not S_4, which is the average site symmetry in the paraelectric phase, as determined by X-ray analysis [5].

At room temperature, the Raman spectrum of Cu-KDP is similar to that of KDP [26, 31]. Figures 4 and 5 show the infrared and Raman spectra of pure KDP, Cu-KDP (1), Cu-KDP (2), Cu-KDP (3), Cu-KDP (4) and Cu-KDP (5). Spectral data and proposed assignment are listed in Tables 2 and 3. The analysis is based on the classical identification of external modes implying the whole lattice network, internal modes of the $(H_2PO_4)^-$ tetrahedra and stretching and bending modes of OH bonds. The attribution is done with respect to the KDP attribution taken from [4, 31, 32] and calculated frequencies of free $(H_2PO_4)^-$ ions.

To calculate the frequencies of the vibrational modes of the H_2PO_4 entity, ab initio RHF/MP2 and DFT/B3LYP electronic structure calculations were carried out using the TZV standard basis set augmented by one diffuse and one polarization functions implemented in the GAMESS program [33]. To identify different vibrational modes, the MOLDEN package [34] was used. Vibrational levels obtained by RHF/MP2 and DFT/B3LYP calculation on free $(H_2PO_4)^-$ and in the experimental result are compared with those measured [32] in aqueous solution.

Figure 6 shows the correlation of the free $(H_2PO_4)^-$ group vibrations in C_{2v} internal vibrations in C_2 factor group symmetry through the D_{2d} one in the crystal.

The spectroscopic characteristics of the free H_2PO_4 ion with pseudo-symmetry C_{2v} can be deduced from the free tetrahedral PO_4 entity. The two stretching modes ν_1 (~938 cm^{-1}) and ν_3 (~1,017 cm^{-1}) lead to four stretching modes (two modes $\nu(PO_2)$, one antisymmetrical (B_1) at about 1,033 cm^{-1} and one symmetrical (A_1) at 1,060 cm^{-1}, and two ν(P $(OH)_2$) around 732 and 759 cm^{-1} with symmetry A_1 and B_2, respectively) (Fig. 6). The bending modes, arising from ν_2 and ν_4, are expected at around 315 and 382 cm^{-1} and at 419, 475 and 484 cm^{-1}, respectively. Finally, the three calculated frequencies involving the OH group are 1,093, 1,299 and 3,830 cm^{-1}. All of these vibrations theoretically appear in Raman spectra, and only the vibrations with symmetry mode A_1, B_1, and B_2 appear in IR spectra.

As shown in Figs. 4 and 5, the additive has a considerable influence in the Raman and IR spectra. For example, the bands which appear at 3,600 and 3268 cm^{-1} in pure KDP and assigned to free O–H stretching [19] are absent from Cu-KDP (3). The absence of these peaks supports the adsorption of Cu^{2+} in the surfaces of the crystal. The deviation of IR frequencies for O–H stretching observed at 3,435 and 3,516 cm^{-1} in pure KDP [19] to higher frequencies, respectively, at 3,483 and 3,565 cm^{-1} in Cu-KDP (3) reflects the possible entry of Cu^{2+} cations in the lattice site of the KDP crystal. The increasing frequency of O–H stretching indicates clearly the weakening of the bond strength between oxygen and hydrogen and the interaction of dopant with P–O–H group of KDP. The entry of Cu^{2+} ions into the lattice of the tetragonal KDP crystal can be also confirmed by the variation of Raman and IR frequencies for stretching and bending vibrations $\nu(PO_2)$,$\nu P(OH)_2$, $\delta(H_2PO_4)$ and $\gamma(H_2PO_4)$ (Tables 2 and 3).

In the Raman spectra, we observed two new bands centred at 253 and 235 cm^{-1} in the spectrum of Cu-KDP (3). We observed that these two peaks become more intense for Cu-KDP (5). These two bands are characteristic of the Cu–O bond [35].

External modes result from translational and vibrational modes of anions and translational ones of cations. The vibrational

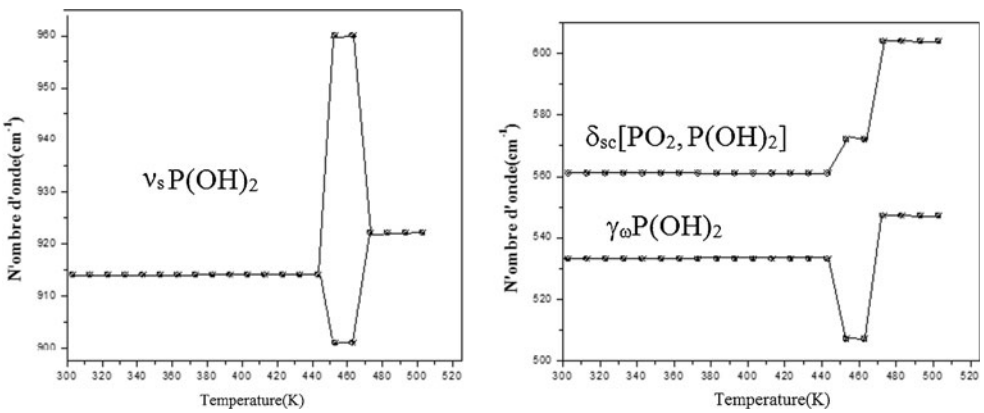

Fig. 10 The temperature dependence of the wavenumbers of some bands observed in the Raman spectra of the Cu-KDP (5)

and translational modes of anions can be seen as hydrogen bond stretchings and bendings inside the layers. They are observed below 300 cm^{-1} for KDP families [36]. According to Som et al., the lines observed at 116 and 154 cm^{-1} in pure KDP and at 118 and 155 cm^{-1} in Cu-KDP may be assigned to K–PO_4 translatory vibrations along the c-axis [37]. The 187 cm^{-1} in Cu-KDP (3) band can be assigned to the H_2PO_4 rotational band. The band observed at 193 cm^{-1} from Cu-KDP (3) can be attributed to the stretching ν(O–H≡O) bridge vibration. This band is observed at about 191 cm^{-1} in Raman spectra of pure KDP.

The ABC-type broad bands of high-frequency H vibrations have been interpreted as O–H stretching modes in Fermi resonance with combination involving mainly O–H bending vibrations [38] or in terms of strong coupling between fast O–H and slow O=O stretching modes [38]. These spectral characteristics have been observed in a variety of strong hydrogen-bonded solids having O–O distances varying from 2.45 to 2.66 Å [39]. In the present case, the ABC-type bands appear in the Raman spectrum of pure KDP at 2,728, 2,370 and 1,817 cm^{-1}, respectively (Fig. 7). These bands appear at about 2,830, 2,383 and 11,758 cm^{-1}, respectively, in Cu-KDP (5) (Fig. 7). The substantial change in the position of these bands reflects the possible incorporation of Cu^{2+} in the lattice site of KDP crystal.

In conclusion, in a low concentration of copper (Cu-KDP (1) and Cu-KDP (2)), all of the copper is practically substituted in volume, whereas in the high concentrations the copper is absorbed in both volume and the surface.

It is reported that at an increase of the temperature above 453 K, a monoclinic phase is obtained. The tetragonal→monoclinic transition usually occurs at a temperature between 453 and 493 K; the measured value depends strongly on sample preparation [8, 40]. In the monoclinic phase, space group $P2_1/m$ (C_{2h}), the atomic distribution and lattice parameters at 463 K are obtained (a=7.590 Å, b=6.209 Å, c=4.530 Å, β=107.36°) [8].

In Fig. 8, the increase of temperature from 303 to 503 K shows some modifications in the Raman spectra of Cu-KDP (5) but

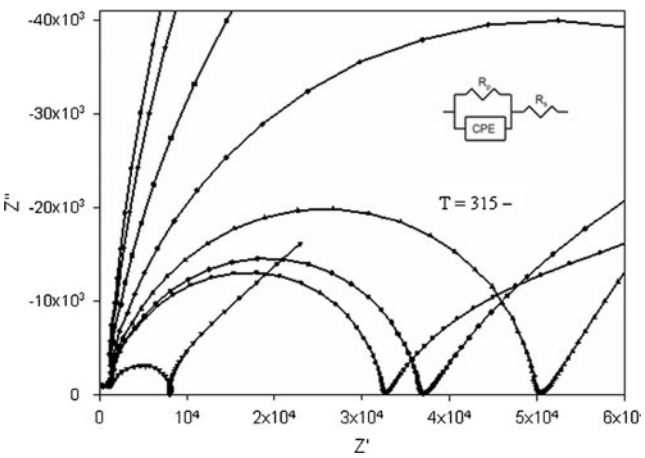

Fig. 11 Complex plane plots of Cu-KDP (5) at various temperatures

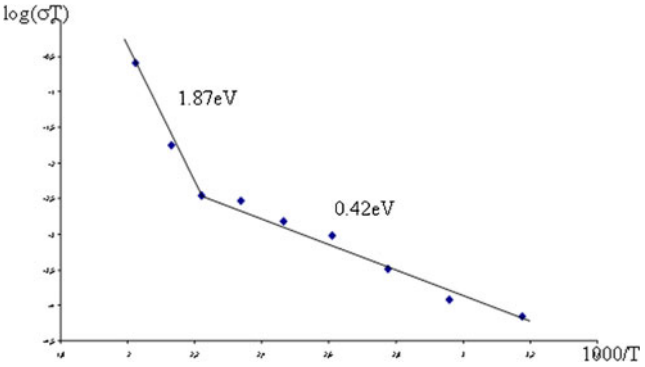

Fig. 12 Conductivity plots log (σT)=f (1,000/T) for Cu-KDP (5) compound

without any well-known bands due to P_2O_7 entities [40]. These bands might indicate some dehydration (Table 4). Two-phase transitions at 453 and 473 K are related to Cu-KDP (5) (Fig. 9).

The increase of temperature in Cu-KDP (5), between 303 and 503 K, causes the disappearance of lines at low frequency, corresponding to the lattice modes and the band at 193 cm^{-1}, attributed to the stretching O==O bridge vibrations. The appearance in Cu-KDP (5) spectrum of a line at 61 cm^{-1} and another at 1,175 cm^{-1} corresponds to $\nu_{as}(PO_2)$ vibrations. Also, there are substantial changes in the position and intensity of some bands corresponding to the internal vibrations of H_2PO_4.

The most important change concerns the Raman line associated to $\nu_{as}P(OH)_2$ mode. This strong line observed at 914 cm^{-1} at room temperature splits to two Raman lines near 901 and 960 cm^{-1} for the temperature between 453 and 463 K and reappears (from 473 K) with a single strong line at 922 cm^{-1}. The frequency of this vibration, $\nu_{as}P(OH)_2$, estimated by Joost Vande Vondele et al. [32] from the calculation of free H_2PO_4 and in aqueous solution are 795 and 944 cm^{-1}, respectively.

Appreciable changes are also observed for lines at 1,175 cm^{-1} due to $\nu_{as}(PO_2)$ vibrations. This line appears between 453 and 473 K and disappears from 483 K.

A plot of the temperature behaviour of some Raman wavenumber is shown in Fig. 10, which unambiguously proves the existence of singularities in the temperature range 303–503 K. From these curves, the temperature of the II→I (a) transition is estimated at 453 and 473 K for I-a→I-b transition.

Table 5 Selected transport properties of Cu-KDP. Activation energies for proton conductivity determined from fit of $\sigma=A/T \exp(-E_a/KT)$ over the temperature range stated. Conductivity given for the temperature listed

Phase	E_a (eV)	T range (K)	Sigma (Ω^{-1} cm^{-1})	T (K)
I(a)	0.42	315–450 K	2.2×10-	315
I(b)	1.87	450–494 K	3.7×10^{-5}	472

Dielectric properties

Some complex impedance diagrams $-Z''$ versus Z' at various temperatures are given in Fig. 10 and show that Cu-KDP (5) follows the Cole–Cole law. The bulk ohmic resistance relative to experimental temperature is the intercept on the real axis of the zero-phase angle extrapolation of the highest frequency curve.

In Fig. 11, the equivalent circuit of the crystal under the ac electric field at lower temperatures can be modelled well as a solution resistance R_s in series with the parallel combination of a polarization resistance R_P with a constant phase angle element (cpe).

The conductivity of Cu-KDP (5) is shown in Arrhenius curve (Fig. 12). Only one transition, at Ttr=450 K, of the two transitions noted by the calorimetric and Raman studies is apparent in the conductivity results. This transition leads to a sharp increase of the conductivity. The second transition is not observed because it produces a small impact on the transport properties.

The activation energies are obtained as E_a=0.42 and 1.87 eV above and below Tp=450 K for the ionic hopping of mobile ions (H^+) (Table 5). In the KDP material, the activation energies are 0.42 and 0.68 eV for the temperature above and below 453 K, respectively. In KH_2AsO_4, the activation energies are 0.40 and 0.59 eV for the temperature above and below 453 K [41].

It is noteworthy that the superprotonic Cu-KDP (5) has a rather low activation energy for proton transport (0.42 eV) and a significantly higher conductivity (2.2×10^{-7} Ω^{-1} cm^{-1}) for the polycrystalline pellet compared to the pure KDP (10^{-10} Ω^{-1} cm^{-1}) [5, 42]. It is possible that the higher conductivity is due to the proton defects in Cu-KDP caused by the substitution of K^+ by Cu^{2+}.

General conclusions

The high temperature phenomena of Cu-KDP are not related to chemical change such as thermal decomposition but related to the physical change of the structural phase transition. Doping KDP with Cu^{2+} significantly modifies its electric properties. The transport properties of protons in such crystals may be treated in terms of proton defects.

Acknowledgments Many thanks to Unité de sepectroscopie Raman FSS Sfax for the measurements of Raman spectra. The authors wish to express their gratitude to Prof. Mohamed Bahri from the Faculty of Science, Sfax, Tunisia, for the calculation of the frequencies of the $(H_2PO_4)^-$ group.

References

1. Park J-H, Kim C-S, Choi B-C, Moon BK, Seo H-J (2003) Physical properties of CsH_2PO_4 crystal at high temperatures. J Phys Soc Jpn 72:1592–1593
2. Li Z, Tang T (2010) High-temperature dehydration behavior and protonic conductivity of RbH_2PO_4 in humid atmosphere. J Mater Res Bull 45:1909–1915
3. Chen RH, Yen C-C, Shern CS, Fukami T (2006) Impedance spectroscopy and dielectric analysis in KH_2PO_4 single crystal. J Solid State Ionics 177:2857,2864
4. Serra KC, Melo FEA, Nendes Fllho J, Germano FA, Morelra JE (1988) Raman study of the tetragonal→monoclinic phase transition in KDP. J Solid State Commun 66:575–579
5. Kawahata Y, Tominaga Y (2008) Dynamical mechanism of ferroelectric phase transition in KDP/DKDP mixed crystals and distortion of PO_4 tetrahedron. J Solid State Commun 145:218–222
6. Asakuma Y, Takeda S, Maeda K, Fukui K (2009) Kinetic and theoretical studies of metal ion adsorption in KDP solution. J Appl Surf Sci 255:4140–4144
7. Ponomareva VG, Martsinkevich VV, Chesalov YA (2011) Transport and thermal characteristics of $Cs_{1-x}Rb_xH_2PO_4$. J Electrochem 47:645–653
8. Botez CE, Carbajal D, Adiraju VAK, Tackett RJ, Chianelli RR (2010) Intermediate-temperature polymorphic phase transition in KH_2PO_4: a synchrotron X-ray diffraction study. J Phys Chem Solids 71:1576–1580
9. Diosa JE, Vargas RA, Albinsson I, Mellander B-E (2004) Dielectric relaxation in single crystal $NH_4H_2PO_4$ in the high-temperature regime. J Solid State Commun 132:55–58
10. Grunberg J, Levin S, Pelah I, Gerlich D (1972) High temperature phase transitions and metastability in KDP type crystals. J Phys Status Solidi 49:857
11. Lee J-K (1996) Hidden nature of the high-temperature phase transitions in crystals of KH_2PO_4 type: is it a physical change? J Phys Chem Solids 57:333
12. Ortiz E, Vargas A, Mellander B-E (1998) On the reported high-temperature phase transition in KH_2PO_4—strong evidence of partial polymerization instead of a structural phase. J Phys Chem Solids 59:305–310
13. Itoh K, Matsubayashi T, Nakamura E, Motegi H (1975) X-ray study of high-temperature phase transitions in KH_2PO_4. J Phys Soc Jpn 39:843–844
14. Vargas RA, Chacon M, Trochez JC (1989) Specific heat of KDP near the tetragonal–monoclinic phase transition. J Solid State Ionics 34:93–95
15. Boysen DA, Haile SM (2004) Conductivity of potassium and rubidium dihydrogen phosphates at high temperature and pressure. J Chem Mater 16:693–697
16. Bronowska W (2006) High-temperature phenomena in RbD_2PO_4 and CsH_2PO_4 polymeric transformations or polymorphic phase transitions? J Mater Sci-Pol 24:230–236
17. Rajesh NP, Kannan V, Santhana Raghavan P, Ramasamy P, Lan CW (2002) Optical and microhardness studies of KDP crystals grown from aqueous solutions with organic additives. J Mater Lett 52:326–328
18. Ogorodnikov IN, Yakovlev VY, Shulgin BV, Satybaldieva MK (2002) Transient optical absorption of hole polarons in ADP ($NH_4H_2PO_4$) and KDP (KH_2PO_4) crystals. J Phys Sol State 44:880–887
19. Kumaresan P, Moorthy Babu S, Anbarasan PM (2008) Growth and characterization of metal ions and dyes doped KDP single crystals for laser applications. J Mater Res Bull 43:1716–1723
20. Bredikhin VI, Galushkina GL, Kulagin AA, Kuznetsov SP, Malshakova OA (2003) Competing growth centers and step bunching in KDP crystal growth from solutions. J Cryst Growth 259:309–320
21. Alexandru HV, Antoh S (1996) Prismatic faces of KDP crystal, kinetic and mechanism of growth from solutions. J Cryst Growth 169:149–157

22. Eremina TA, Kuznetsov VA, Eremin NN, Okhrimenko TM, Furmanova NG, Efremova EP, Rak M (2005) On the mechanism of impurity influence on growth kinetics and surface morphology of KDP crystals—II: experimental study of influence of bivalent and trivalent impurity ions on growth kinetics and surface morphology of KDP crystals. J Cryst Growth 273:586–593
23. Eremina TA, Eremin NN, Furmanova NG, Kuznetsov VA, Okhrimenko TM, Urusov VS (2001) Simulation of a defect region in KDP crystals doped with divalent iron ions. Comparison of defects induced by di- and trivalent metals. J Crystallogr Rep 46:75–80, Translated from Kristallografiya, Vol. 46(2001), pp. 82, 87
24. Eremina TA, Eremin NN, Kuznetsov VA, Furmanova NG, Urusov VSJ (2002) Simulation of defects formed by cations of bivalent and trivalent metals in the structure of potassium dihydrogen phosphate: a computational technique. J Crystallogr Rep 47:753–758, Translated from Kristallografiya. 47 (2002), pp. 819, 824
25. Toumi M, Mhiri T, Bulou A (2009) Raman spectroscopic study of $K_3H(SO4)_2$ (phases I and II) single crystals. J Vib Spectrosc 50:298–302
26. Lu G, Li C, Wang W, Wang Z, Guan J, Xia H (2005) Lattice vibration modes and thermal conductivity of potassium dihydrogen phosphate crystal studying by Raman spectroscopy. J Mater Sci Eng 116:47–53
27. Li G, Liping X, Su G, Zhuang X, Li Z, He Y (2005) Study on the growth and characterization of KDP-type crystals. J Cryst Growth 274:555–562
28. J. Rodriguez-Carvajal (2005) Program FULLPROF, version 2.6.1
29. Nelmes RJ (1987) Ferroelectrics 71:87
30. Help menu on equivalent circuits, instant curve fitting function and constant phase element in the ZView program (ver. 3.2c) from Scribner Associates, Inc
31. Videnova-Adrabińska V, Wojciechowski W, Baran J (1987) Polarized infrared and raman spectra of monoclinic CsH_2PO_4 single crystal and its deuterated homologue CsD_2PO_4: part II. Internal vibrations of the PO_4 ion. J Mol Struct 156:15–27
32. Vondele JV, Tröster P, Tavan P, Mathias G (2012) Vibrational spectra of phosphate ions in aqueous solution probed by first-principles molecular dynamics. J Phys Chem 116:2466–2474
33. Schmidt MW, Baldridge KK, Boatz JA, Elbert ST, Gordon MS, Jensen JH, Koseki S, Matsunaga N, Nguyen KA, Su SJ, Windus TL, Dupuis M, Montgomery JA (1993) General atomic and molecular electronic structure system. J Comput Chem 14:1347–1363
34. Schaftenaar G, Noordik JH (2000) Molden: a pre- and post-processing program for molecular and electronic structures. J Comput Aided Mol Des 14:123,134
35. Vedeanu N, Cozar O, Ardelean I, Lendl B (2006) IR and Raman investigation of $x(CuO \cdot V_2O_5)(1-x)[P_2O_5 \cdot CaF_2]$ glass system. J Optoelectron Adv Mater 8:78,81
36. Lee K-S, Ko J-H, Moon J, Lee S, Jeon M (2008) Raman spectroscopic study of LiH_2PO_4. J Solid State Commun 145:487–492
37. Som T, Navati MS, Kulkarni VN (2001) Physico-chemical changes in ion-irradiated KDP. J Nucl Inst Methods Phys Res 179:551–556
38. Choi B-K (1995) High temperature phase transition and thermal decomposition of KH_2PO_4 crystals. J Phys Chem Solids 56:1023–1030
39. Taher LB, Chabchoub S, Smiri-Dogguy L (1999) Investigation of mixed alkaline earth phosphates. Synthesis and crystal structure of $CaBa(HPO_4)_2$: a new mixed alkaline earth hydrogenmonophosphate. J Solid State Sci 1:15–24
40. Park J-H (2002) Separation of surface and bulk electrical conductivity in KH_2PO_4 and KH_2AsO_4 crystals at high temperatures. J Solid State Commun 123:291–294
41. Mathew M, Wong-Ng W (1995) Crystal structure of a new monoclinic form of potassium dihydrogen phosphate containing orthophosphacidiumion, $[H_4PO_4]^{+1}$. J Solid State Chem 114:219–223
42. Kim SH, Lee KW, Kim I-M, Lee CE (2006) Impedance study near the ferroelastic transition in TlH_2PO_4. J Appl Phys Lett 88:192901